ARID ZONE JOURNAL OF ENGINEERING, TECHNOLOGY & ENVIRONMENT
AZOJETE September 2025. Vol.21(3):868-879
Published by the Faculty of Engineering, University of Maiduguri, Maiduguri, Nigeria.
Print ISSN: 1596-2490, Electronic ISSN: 2545-5818
https://doi.org/10.63958/AZOJETE/2025/21/03/017
www.azojete.com.ng

ORIGINAL RESEARCH ARTICLE

SPRAY DRYING MODELLING USING ADVANCED VAPORIZATION APPROACH

A. BELLO[1*], B. R. ADEMOLA[2], AND U. A. ISAH[2]

[1]*Department of Chemical Engineering, University of Maiduguri, Borno State, Nigeria*
[2]*Department of Chemical Engineering, University of Port Harcourt, Rivers State, Nigeria*
**Corresponding author: aliyub@unimaid.edu.ng*

ARTICLE INFORMATION

Received: 8th September 2025
Revised: 14th September 2025
Accepted: 16th September 2025

Keywords:
Juice
Spray drying
Modelling
Advanced droplet vaporization
Moisture content

ABSTRACT

This study develops a deterministic mathematical model for simulating the spray drying of pineapple juice. The model applies advanced vaporization kinetics and a receding interface-porous diffusion approach to predict moisture content, droplet density, and temperature. Validated experimentally at feed solids concentrations of 20% and 40% and drying temperatures of 130 °C and 140 °C, the model accurately predicted final moisture content with absolute errors ranging from 2.3% to 5.2% as drying gas temperature decreases from 140 °C to 130 °C for the 20% feed, and from 1% to 1.8% for the 40% feed. Key results quantitatively demonstrate that higher air temperatures reduce final moisture content and reveal the critical role of crust formation in shifting the drying kinetics from a rapid evaporation phase to a slower, diffusion-limited regime. The model's computational efficiency and physics-based foundation make it a valuable tool for the optimization of spray drying processes, potentially reducing reliance on costly and time-consuming experimental trials.

1.0 Introduction

Spray drying process accounts for a significant volume of dry powder production globally. It is used to produce instant products such as fruit juice powder, egg powder, coffee, tea extract, honey powder, milk, flavours, soup powders, baby milk formula, spices and herb extracts, cheese powder, yogurt powder, and vegetable powders (Barbosa-Cánovas *et al.* 2006; Filkova *et al.* 2014). Droplet drying kinetics models are indispensable in modelling the spray drying of droplets. Four primary models are documented in literature. The Characteristic Drying Curve (CDC) model relies on semi-empirical drying curves from experimental data. While computationally efficient, its accuracy diminishes when applied to conditions different from the original experiments (Mezhericher *et al.* 2010; Poozesh *et al.* 2018). The Reaction Engineering Approach (REA) uses an empirical correlation between particle solvent content and partial vapor pressure, framing evaporation as an activation energy barrier. However, its predictive capability is limited to materials with pre-existing experimental data for correlation, as the activation energy is highly specific to both the material and the drying conditions (Chen and Putranto 2015; Putranto and Chen 2015). Deterministic models are based on fundamental heat and mass transfer equations to account for internal gradients. However, they can be computationally expensive due to moving boundaries (e.g., tracking a receding wet core interface) and require numerous precise input parameters (e.g., mass diffusivity, porosity) which limits their practical application (Boel *et al.* 2020; Razmi *et al.* 2021). Accurate Computational Fluid Dynamics (CFD) models resolve three-dimensional chamber hydrodynamics, turbulence, and droplet-gas interactions. Their key limitations are prohibitive computational cost. Additionally, they still rely on accurate sub-models for droplet drying kinetics and wall interactions to be predictive (Boel *et al.* 2020; Razmi *et al.* 2021).

Therefore, a clear need exists for a mechanistic model that is both predictive and computationally efficient, without relying on empirical drying parameters. This study advances a deterministic mathematical model of spray drying using the advanced droplet vaporisation kinetics and receding interface-porous diffusion approach (Sazhin *et al.* 2013; Werner *et al.* 2008). The droplet vaporisation approaches of Sazhin (2006) and Abramzon and Sirignano (1989) provide a basis for understanding droplet dynamics and evaporation and their approach will be coupled with interface-porous diffusion to examine the evaporation of droplets containing multiple

components. The novelty of this work lies in the integrated application and validation of this coupled model for a complex, multi-component food system (pineapple juice-maltodextrin), with a focus on achieving predictive accuracy for key outputs like final moisture content while maintaining computational efficiency for engineering design.

2. Materials and Methods

2.1. Theoretical Approach and Model Equations

Studies of droplet drying into dry particles show two distinct drying steps that may be preceded or concluded by heating. It is assumed the drying droplets have a spherical shape and possess uniform composition, thermal properties, and shrinkage (Mezhericher *et al.* 2014; Sadafi *et al.* 2014). The typical multicomponent juice feed is made up of liquid with solids (dissolved and micro solids) which is atomized into a stream of hot gas as a spray of fine droplets. Heat transfer takes place between the droplets and the hot gas stream, leading to the evaporation of liquid from the droplet surface. As the droplet evaporates, it undergoes shrinkage and becomes increasingly viscous due to the reduction in its liquid content. The rate at which liquid flows from the interior of the viscous droplet to its surface decreases as the evaporation progresses and the droplet continues to shrink. At a critical droplet diameter, marking end of the first drying step, surface evaporation rate will exceed the rate of liquid flow from viscous droplet interior to surface and a crust layer forma, that grows inwards. The crust layer fixes the droplet diameter and marks the transition into a wet particle whereby heat conducts through the crust to evaporate pore liquid which, flow gaseous through the dry crust to the surface. The complete evaporation of pore liquid ends the second drying step and transforms the wet particle into a dry one that steadily and uniformly heats up before exit from the spray dryer. The model initial droplet evaporation stage is governed by the advanced vaporization kinetics of Abramzon and Sirignano (1989), which provides an accurate account of heat and mass transfer by incorporating the blowing effect of high evaporation rates. This represents an advancement over simpler correlations often used in food powder modelling. The model then seamlessly couples to a receding interface-porous diffusion model, to simulate the second drying stage once a solid crust forms. This hybrid approach allows the model to leverage the strengths of the physical precision of combustion droplet models for the initial phase and the practical relevance of food powder models for the important crust-drying phase.

2.1.1. Droplet motion and trajectory

Atomized spherical droplets numbering $\dot{N}$, ejected from an atomizer with initial velocity U [m s^{-1}], have their motion and trajectory inside the spray drying chamber defined by drag and body forces and flow turbulence. Assuming that the droplets follow vertical trajectories from the atomizer exit to the bottom of the spray drying chamber without any interaction with the walls, the body forces acting on the droplets are the combined effect of gravitational force and buoyant force resulting from volume displacement and are given by Equation 1:

$$\vec{F}_{body} = \left(\rho_d - \rho_g\right)\vec{g}\,\frac{\pi}{6}D_d^3 \qquad 1$$

Where $\vec{F}_{body}$ = body forces acting on droplet [N], D = diameter [m], $\vec{g}$ = gravitational acceleration [9.81 m s^{-2}], ρ = density [kg m^{-3}], and subscripts d and g refer to droplet and gas respectively. The aerodynamic drag forces are given by Equation 2:

$$\vec{F}_{drag} = -\frac{1}{2}\rho_g\left|U_d - U_g\right|\left(U_d - U_g\right)A_d C_d \qquad 2$$

Where $\vec{F}_{drag}$ = aerodynamic drag forces [N], A = area [m^2], and C_d = dimensionless drag coefficient. The droplet area for the drag calculation is obtained from Equation 3:

$$A_d = \frac{pi}{4}D_d^2 \qquad 3$$

The drag coefficient C_d is influenced by the relative velocity of the droplet and the Reynolds number. For accurate predictions in Reynolds flow regimes involving moving and evaporating droplets, the correlation developed by Feng and Michaelides (2001) is applied. This approach accounts for the effects similar to that in spray dryers (Michaelides 2013; Sazhin 2006). Thus, the C_d is calculated using the following correlations for the flow regimes, using Equation 4:

Corresponding author's email address: aliyub@unimaid.edu.ng

$$C_D = \begin{cases} \frac{2-\gamma}{2} C_{d0} + \frac{4\gamma}{6+\gamma} C_{d2} & 0 \le \gamma \le 2, \text{ and } 5 < \mathrm{Re}_d \le 1000 \\ \frac{4}{\gamma+2} C_{d2} + \frac{\gamma-2}{\gamma+2} C_{d\infty} & 2 \le \gamma \le \infty, \text{ and } 5 < \mathrm{Re}_d \le 1000 \\ \frac{8}{\mathrm{Re}_d} \frac{3\gamma+2}{\gamma+1} \left(1 + 0.05 \frac{3\gamma+2}{\gamma+1} \mathrm{Re}_d\right) - 0.01 \frac{3\gamma}{\gamma+1} \mathrm{Re}_d \ln \mathrm{Re}_d & 0 \le \mathrm{Re}_d \le 5 \end{cases} \quad (4)$$

Where γ = viscosity ratio and Re_d = droplet dimensionless Reynolds number. And we have,

$$\gamma = \frac{\mu_d}{\mu_g} \quad (5)$$

$$\mathrm{Re}_d = \frac{|U_d - U_g| \rho_g D_d}{\mu_g} \quad (6)$$

Where μ = viscosity [N s/m^2]. The C_{d0}, C_{d2}, $C_{d\infty}$ functions in Equation 4 were given by Feng and Michaelides (2001) and are expressed in Equation 7, 8 and 9 respectively:

$$C_{d0} = \frac{48}{Re_d} \left(1 + \frac{2.21}{\sqrt{Re_d}} - \frac{2.14}{Re_d}\right) \quad (7)$$

$$C_{d2} = 17.0 Re_d^{-2/3} \quad (8)$$

$$C_{d\infty} = \frac{24}{Re_d} \left(1 + \frac{1}{6} Re_d^{2/3}\right) \quad (9)$$

When the Reynolds flow regimes exceed 1000, a different correlation for the drag curve for solid spheres by Morrison (2013) which is used in a form given by Equation 10:

$$C_D = \frac{24}{\mathrm{Re}_d} + \frac{2.6\left(\frac{\mathrm{Re}_d}{5.0}\right)}{1 + \left(\frac{\mathrm{Re}_d}{5.0}\right)^{1.52}} + \frac{0.411\left(\frac{\mathrm{Re}_d}{263000}\right)^{-7.94}}{1 + \left(\frac{\mathrm{Re}_d}{263000}\right)^{-8.0}} + \left(\frac{\mathrm{Re}_d^{0.8}}{461000}\right) \quad (10)$$

The balance of drag and body forces is then calculated from Equation 11:

$$\frac{dU_d}{dt} = \left(\frac{1}{\rho_d \frac{\pi}{6} D_d^3}\right) \left(\vec{F}_{body} + \vec{F}_{drag}\right)$$

The droplets vertical position from the atomizer exit is given by Equation (12):

$$\frac{dh_x}{dt} = U_d \quad (12)$$

where h_x = vertical distance travelled by droplet = drying chamber section height [m].

2.1.2 Droplet mass balance

The sprays of droplets undergo evaporation along their trajectories through the spray dryer length. Assuming saturated conditions at the droplet surface, uniform droplet shrinkage, no wall deposition, well-mixed gas phase and no reaction, the extended film diffusional mass transfer rate from a stagnant droplet in quiescent air is given by Sazhin (2014), as shown in Equation 13:

$$\dot{m}_v = 2\pi D_d \left(\frac{\bar{k}}{\bar{C}p}\right)_g \ln\left(1 + B_M\right) \quad (13)$$

Where $\dot{m}_v$ = vapour mass flow rate [kg s^{-1}], C_p = specific heat [J kg^{-1} K^{-1}], B_m = Spalding mass transfer number and $\bar{k}$ = thermal conductivity [W m^{-1} K^{-1}]. A correction factor is needed for the convective effects of the

Corresponding author's email address: aliyub@unimaid.edu.ng

relative velocity between droplet and air which is applied to Equation 13. Thus, the mass balance over a droplet is expressed by Equation 14 (Abramzon and Sirignano 1989; Sazhin 2006):

$$\dot{m}_v = \pi D_d \left(\frac{\bar{k}}{\bar{C}p}\right)_g Sh^* \ln(1+B_M) \quad 14$$

Sh^* = dimensionless modified Sherwood coefficient. Blowing effects are accounted by the modified Sherwood coefficient which, is computed in the manner set out by Abramzon and Sirignano (1989) from Equation 15:

$$Sh^* = 2 + \frac{(Sh_d - 2)}{F_M} \quad 15$$

Where Sh_d = droplet dimensionless Sherwood coefficient and F_m = dimensionless blowing effect correction factor. F_m is defined by Equation (16):

$$F_M = (1+B_M)^{0.7} \frac{\ln(1+B_M)}{B_M} \quad 16$$

The change in droplet mass is obtained by difference while the decreased droplet radius as a result of moisture loss is obtained from the mass-volume balance from Equation 17:

$$\frac{dR_d}{dt} = -\frac{\dot{m}_v}{\rho_w \pi D_d^{\,2}} \quad 17$$

Where R = radius [m] and subscript w refers to water. The new moisture content of each droplet on a dry basis is calculated from Equation 18:

$$X_{db} = \frac{m_d}{m_z} \quad 18$$

Where X_{db} = droplet moisture content on dry basis, m = mass [kg] and subscript z refers to solids in droplet. The total mass of evaporated moisture from the spray of droplets is obtained from Equation 19:

$$m_v = \dot{N}\dot{m}_v dt \quad 19$$

Where m_v =mass of moisture loss from droplet.

2.1.3. Droplet heat balance

The energy for moisture evaporation and temperature rise in the droplets is provided from conduction across the droplet surface from the drying gas (Gopireddy and Gutheil 2013; Sazhin *et al.* 2011) The total energy balance over a droplet is calculated from Equation 20:

$$Q_d = \pi D_d Nu^* \bar{k}_g (T_\infty - T_{d,s}) \quad 20$$

Where Q = rate of heat transfer [J s^{-1}], Nu* = modified Nusselt number, T = temperature [K], and subscript d,s refers to droplet surface. The modified Nusselt number is computed from Equation 21 (Sazhin 2006):

$$Nu^* = 2 + \frac{(\mathrm{Nu}_d - 2)}{F_H} \quad 21$$

Where F_H = thermal film thickness correction factor and Nu = Nusselt number. The thermal film thickness correction factor is obtained from Equation 22 (Sazhin 2006):

$$F_H = (1+B_H)^{0.7} \frac{\ln(1+B_H)}{B_H} \quad 22$$

Where B_H = Spalding heat transfer coefficient. The mean droplet temperature is obtained from Equation 23:

$$\frac{dT_d}{dt} = \frac{Q_d - \dot{m}_v \Delta L_v(T_d)}{m_d(W_z Cp_z + W_w Cp_w)} \quad 23$$

Where ΔL_v = Latent heat of moisture vaporization [J kg–1], and W = mass fraction.

2.1.4. Wet particle mass balance

The diameter of the evaporating droplets continues to decrease until the critical diameter is reached. The dry formed crust is assumed to form uniformly round the droplet liquid core and then gradually grow inwards as the liquid core evaporates. The critical diameter depends on the porosity of the growing layer of dry crust and is determined from Equation 24:

$$D_{d,cr} = \sqrt[3]{\left(\frac{6V_z}{1-\psi}\right) / \, pi} \quad 24$$

Where V = volume [m^3], ψ = particle porosity and subscript cr = critical droplet diameter for crust formation. On formation of the dry surface crust layer, droplets transit into wet particles with a receding wet core and a radially growing dry crust surface. The moisture evaporation from a wet particle occurs via evaporation at

Corresponding author's email address: aliyub@unimaid.edu.ng

the wet core-crust interface surface followed by diffusion and flow through the porous crust. The moisture loss from a droplet is obtained from Equation 25 (Kadja and Bergeles 2003; Mezhericher *et al.* 2007):

$$\frac{dm_v}{dt} = -\left[\frac{8\pi\psi^m D_{WA,c} W_w \bar{\rho}_g}{\Re\left(T_{p,s}+T_{wc,i}\right)}\left(\frac{D_p D_{wc}}{D_p - D_{wc}}\right)\right]\ln\left(\frac{\mathrm{p}_g - p_{v,i}}{\mathrm{p}_g - \left(\frac{\Re T_{p,s}\dot{m}_v}{\pi h_M D_p^2} + \frac{p_{v,\infty} T_{p,s}}{T_g}\right)}\right) \quad 25$$

Where the superscript *m* is an empirical coefficient, D_{WA} = diffusion coefficient of water vapor in air [$m^2\ s^{-1}$], h_M = mass transfer coefficient [$m\ s^{-1}$], P = total pressure [Pa], *p* = partial moisture vapor pressure [Pa], $\Re$ = universal molar gas constant [$J\ mol^{-1}\ K^{-1}$], The subscripts *c, i, p, wc,* and *v* respectively mean *crust*, *evaporation interface*, *particle*, *wet core* and *water vapour*. The new radius of the receding wet core interface in the wet particles is tracked using Equation 26:

$$\frac{dR_{wc}}{dt} = -\frac{\dot{m}_v}{\psi\rho_{w,cr}\pi D_{wc}^{\ 2}} \quad 26$$

2.1.5. Wet particle heat balance

The temperature at the wet particle crust surface is given by Equation 27 (Kadja and Bergeles 2003):

$$T_{d,s} = T_{wc} + \pi D_p Nu^* \bar{k}_g \left(T_\infty - T_{d,s}\right)\left(\frac{D_p - D_{wc}}{4\pi D_p D_{wc} k_{cz}}\right) \quad 27$$

Where subscript *cz* denotes *crust solids*. The particle liquid core temperature, T_{wc} is calculated from Equation 28:

$$m_d\left(w_z Cp_z + w_w Cp_w\right)\frac{dT_{wc}}{dt} = \frac{T_{d,s} - T_{wc}}{\frac{D_p - D_{wc}}{4\pi D_p D_{wc} k_{cz}}} - \dot{m}_v \Delta L_v\left(T_{wc}\right) \quad 28$$

2.1.6. Dry particle heat balance

The complete removal of moisture generates dry particles which exchange energy with the drying gas. An energy balance about the particle surface gives its temperature using Equation 29:

$$\frac{dT_p}{dt} = \frac{\pi D_p \mathrm{Nu}\left(T_\infty - T_p\right)k_g}{\left(m_z Cp_z\right)} \quad 29$$

2.1.7. Drying chamber energy and mass balances

The transient changes in mass and energy of the drying gas, as the droplets dry into particles, is obtained from a balance over the time dependent, vertical position of the droplets inside drying chamber (Ali *et al.* 2014). The change in absolute humidity of the drying gas is given by Equation 30 (Masters 1991):

$$AH_n = \frac{F_e\left(X_{db,n-1} - X_{db,n}\right) + G_{n-1}AH_{n-1}}{G_n} \quad 30$$

Where *AH* = humidity (absolute) of gas, F_e = mass flow rate of the atomized feed into the drying chamber section [$kg\ s^{-1}$], and G = dry air mass flow rate [$kg\ s^{-1}$]. Subscripts n (0 to l) denotes *section top (inlet)* position and *bottom (outlet)* respectively. The drying chamber is modelled as a vertical cylinder divided into sections. The heat loss from the chamber section wall is given by Equation 31:

$$W_{hl} = U_{ch} A_{cho} \Delta T_{\mathrm{lg}\,m} \quad 31$$

Where *Whl* = heat loss through drying chamber wall [J], A_{cho} = external heat loss surface area of chamber section, U_{ch} = overall chamber wall external heat transfer coefficient [$J\ s^{-1}\ m^{-2}\ K^{-1}$] and subscript *lgm* means *log mean*. The external spray drying chamber section wall surface area is given by:

Corresponding author's email address: aliyub@unimaid.edu.ng

$$A_{cho} = \pi h_x \frac{D_{cho}}{2} \quad (32)$$

And the log mean temperature difference (LMTD) from:

$$\Delta T_{lgm} = \frac{\left(T_{g,0} - T_{amb}\right) - \left(T_{g,1} - T_{amb}\right)}{\log\left(\frac{\left(T_{g,0} - T_{amb}\right)}{\left(T_{g,1} - T_{amb}\right)}\right)} \quad (33)$$

Where subscripts *amb*, 0 and 1 denote *ambient air*, *chamber section entry* and *chamber section exit* respectively. The convective surface heat transfer coefficient for the internal chamber wall is obtained from the Nusselt coefficient using Equation 34 (Gnielinski 2010):

$$h_{T,chi} = \frac{\mathrm{Nu}_{chi} k_g}{D_{chi}} \quad (34)$$

Where h_T = heat transfer coefficient [W m^{-2} K^{-1}] and subscript *chi* means *internal chamber wall surface*. The Nusselt number for heat transfer from gas to internal wall is calculated from Equation 35:

$$\mathrm{Nu}_{chi} = \frac{(\xi/8)\,\mathrm{Re}_{chi}\,\mathrm{Pr}}{1 + 12.7\sqrt{\xi/8}\left(\mathrm{Pr}^{2/3} - 1\right)}\left[1 + \frac{1}{3}\left(\frac{D_{chi}}{l_{ch}}\right)^{2/3}\right] \quad (35)$$

$$\xi = \left(1.8 \log \mathrm{Re}_{chi} - 1.5\right)^{-2} \quad (36)$$

Where l_{ch} = distance from drying gas entrance point [m], and Pr = Prandtl number. The drying gas temperature is obtained from the energy balance in Equation 37:

$$G_0\left[(1 + AH_0)Cp_g(T_{g,0})T_{g,0} - (1 + AH_1)Cp_g(T_{g,1})T_{g,1}\right] =$$

$$F\left[\left(1 + X_{db,1}\right)Cp_{d,1}T_{d,1} - \left(1 + X_{db,0}\right)Cp_{d,0}T_{d,0}\right] + \Delta L_v m_v + W_{hl} \quad (37)$$

The specific heat of the droplets, inclusive of moisture and solids, is calculated from Equation 38:

$$Cp_{d,n} = \left(1 - w_{w,n}\right)Cp_z(T_{d,n}) + w_{w,n}Cp_w(T_{d,n}) \quad (38)$$

2.2 Juice Spray Drying Experiment

A laboratory-scale spray dryer, shown in Figure 1, was utilized for the spray drying process of pineapple juice feed. To prepare the feed mixture, ripe pineapples (*smooth cayenne cultivar*) were cleaned, and juiced. The extract was then filtered through a 35-mesh kitchen sieve. The moisture content of the juice was determined using a moisture analyser (Ohaus model MB25). Maltodextrin was added in precise calculated amounts to achieve desired feed solids contents of 20% and 40% from Equation 39:

$$m_{de} = \left(\left(\frac{\frac{1 - w_j}{1}}{\frac{1}{w_f} - 1}\right) - w_j\right) \times \text{juice mass} \quad (39)$$

Where m_{de} = required maltodextrin mass; w_j and w_f = solid weight fractions of juice and desired feed. The spray drying configuration involved concurrent flow, where the atomized feed and drying air moved from top to bottom. The drying air supply is passed through a filter to remove any suspended particles before reaching the atomizer and air heater. The compressed air used for drying was heated by an electric resistance heater in the air heater before being supplied to the drying chamber. Within the drying chamber, the pineapple-maltodextrin feed was continuously agitated using a magnetic stirrer and then fed into the chamber through a hygienic pump (Masterflex model 7518-10), where it was atomized into a spray of droplets using a twin-fluid atomizer. Table 1 presents the juice spray drying conditions in more detail. Drying air temperatures of 130 °C and 140 °C were experimentally determined to produce dry powder. The resulting product powders, for the different drying conditions, were collected from the collector at the base of the cyclone. The powder moisture content was automatically determined as weight percent of the dry material, using the moisture

Corresponding author's email address: aliyub@unimaid.edu.ng

analyser, at a temperature of 75 °C. Averaged values of triplicate sample measurements of the moisture content were calculated and expressed in % kg H_2O/kg dry solids (dry basis).

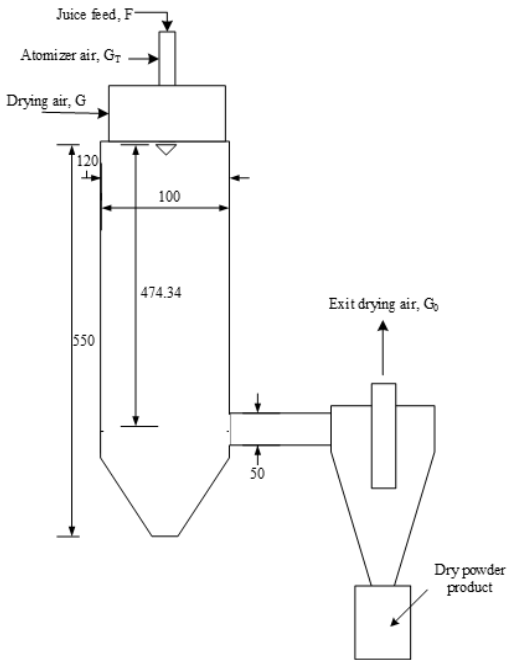

Figure 1: Spray dryer schematic diagram

Table 1: Juice spray drying experiment data

Feed solids fraction	Feed temperature (°C)	Feed Viscosity (Ns/m^2)	Specific gravity (30 °C/30 °C)	Drying air temperature (°C)	Drying air flow rate (L/min)	Drying air humidity (kg H_2O/kg air)
20	29	0.0157	1.043	130	340	0.00506
20	28.5		1.043	140	360	0.00533
40	29		1.095	130	340	0.00512
40	29		1.095	140	342	0.00532

2.3. Spray Drying Model Simulation

The system of coupled ordinary differential equations developed in section 2.1 was solved numerically in MATLAB using a variable-step, 4th-order Runge-Kutta (ode45) solver due to its high-order accuracy which is essential for resolving the model's rapid transients (Akinsola 2023; Semenova *et al.* 2021). The relative and absolute error tolerances for the solver were set to 1×10^{-6} to ensure a precise solution. A maximum time step of 2.5 milliseconds was enforced to resolve the rapid initial transients accurately. The model developed in this study adopts a one-dimensional (1D) plug-flow framework for the drying chamber. The 1D plug-flow assumption is a well-established simplification for tall, concurrent-flow dryer (Razmi *et al.* 2021). The drying chamber was modelled as a one-dimensional plug flow dryer, with the vertical sections from the atomiser determined from Equation 12. The initial conditions for the droplets were based on the twin-fluid atomizer characteristics; the average initial droplet diameter and velocity were calculated from Lorenzetto and Lefebvre Sauter Mean Diameter (SMD) equation (Camacho-Lie *et al.* 2023). The model simulated a single droplet trajectory to represent the average behaviour of the spray with extensive variables calculated for the droplet population. Convergence was assumed when the relative change in all state variables (moisture content, temperature, and diameter) between iterations was less than the specified tolerance. The model is computationally fast, converging averagely in 28s on an I7 8GB RAM laptop. The code takes the initial process conditions, calculates droplet vertical trajectory and then solves the coupled heat and mass transfer equations. The evaporating water properties and constant drying air psychometric properties were calculated using the CoolProp 6.1 module (Bell *et al.* 2014). Sucrose and maltodextrin properties were taken from Adhikari *et al.* (2003). Other required values were obtained from American Society Of Heating, Refrigerating and Air-Conditioning Engineers (ASHRAE) (American society of heating 2013) and IAPWS (Herrmann *et al.* 2011;

Corresponding author's email address: aliyub@unimaid.edu.ng

Pátek *et al.* 2009) correlations which, were implemented in the MATLAB code, are presented in Table 3. The initial calculated droplet sizes and run times are presented Table 2.

Table 2: Initial calculated droplet SMD and simulation runtime

Feed solids fraction	Drying air temperature (°C)	Calculated droplet SMD size (μm)	Simulation run time (s)
20	130	79	28
20	140	95	27
40	130	56	29
40	140	101	29

Table 3: Properties, latent heat and diffusivity correlation used in the model simulation

Parameter	Value	Units
Density		
Maltodextrin	1400	kg m^{-3}
Sucrose	1590	kg m^{-3}
Molar mass		
Water	0.018015268	kg mol^{-1}
Porosity		
Crust porosity	0.38	
Specific heat capacity		
Maltodextrin	3.5242T+1319.7	J kg^{-1} K^{-1}
Sucrose	4.4369T+1121.3	J kg^{-1} K^{-1}
Thermal Conductivity		
Chamber wall (Pyrex glass)	0.96	W m^{-1} K^{-1}
Maltodextrin	0.187	W m^{-1} K^{-1}
Sucrose	0.277	W m^{-1} K^{-1}
Other parameters		
Molar gas constant	8.314462	J mol^{-1} K^{-1}
Water latent heat	$1.91846\times10^{6}\times(T/(T-33.91))^{2}$	J kg^{-1}
Water vapor diffusivity in air	$-2.775\times10^{-6}+4.479\times10^{-8}T+1.656\times10^{-10}T^{2}$	m^2 s

3. Results and discussion

Several variables were tracked during the simulation which, are reported and discussed. Figure 2 presents the average droplet temperature profiles. The trend shows the juice droplets rapidly increase in temperature before decreasing. The increase in droplet temperatures follows the increase in heat and mass transfer rates arising from the initial droplet velocities and hot drying gas temperatures. As heat transfers from the hot gas to the droplet, the juice droplets experience a temperature rise, reaching approximately 50% of the inlet gas temperature. The maximum temperature rise attained by the droplets, a short distance into drying chamber, marks the point at which a crust layer begins to form over the droplet thereby reducing heat transfer and droplet temperature (Bhattacharjee and Gnanaskandan 2023; Rezaei and Netz 2021). After the complete evaporation of the core moisture, the now-dry particle heats rapidly towards the gas temperature. This detailed thermal profile, particularly the internal gradient, demonstrates the model's utility in capturing coupled heat and mass transfer limitations.

Figure 3 illustrates the corresponding evolution of droplet/particle density. The density increases sharply due to the loss of water mass and the concomitant reduction in droplet volume. Upon crust formation, the particle volume becomes fixed. The subsequent gradual decrease in density is solely due to the continued loss of mass (moisture) from within this fixed volume. Figure 4 shows the predicted normalized moisture content and the as a function of residence time along the spray dryer. The drying profile exhibits two distinct falling rate periods, consistent with theory. An initial rapid drying phase is characterized by moisture evaporation from the saturated droplet surface and significant droplet shrinkage. The transition to Period II is marked by the predicted formation of a rigid porous crust, which fixes the particle diameter and impedes moisture removal. This occurs within the first 2% to 3.5% of the distance into the drying chamber. Subsequently, evaporation occurs from a receding wet core interface, and vapor must diffuse through the dry crust layer, leading to a

Corresponding author's email address: aliyub@unimaid.edu.ng

significantly reduced drying rate. Thereafter, the rate then increases again as shown in the lower section of the profile, before the particle exits the drying chamber.

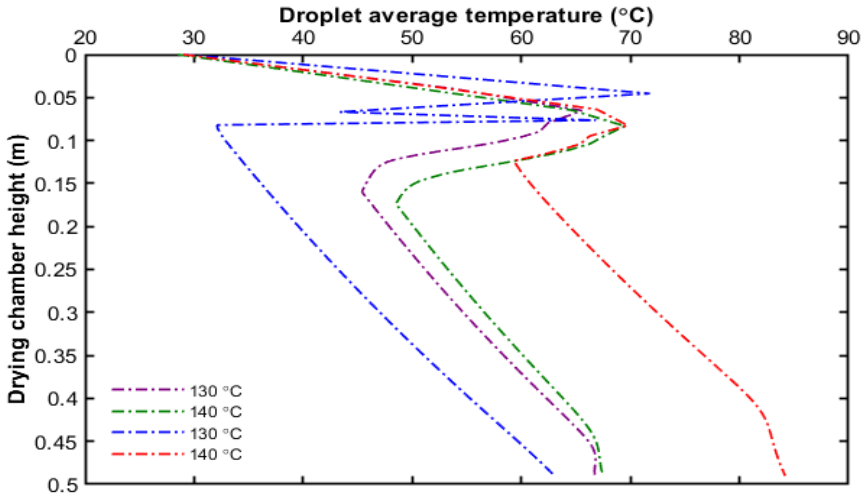

Figure 2: Model simulation results for average droplet temperature

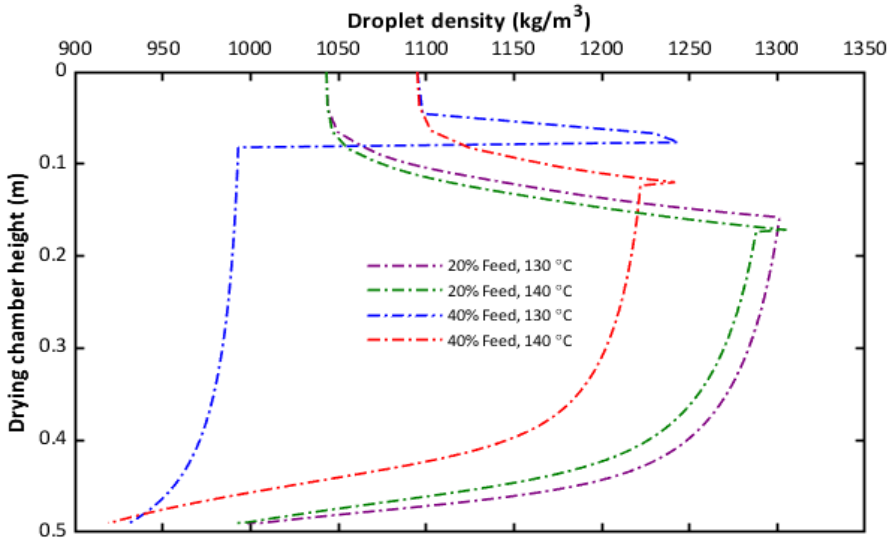

Figure 3: Model simulation results for droplet density

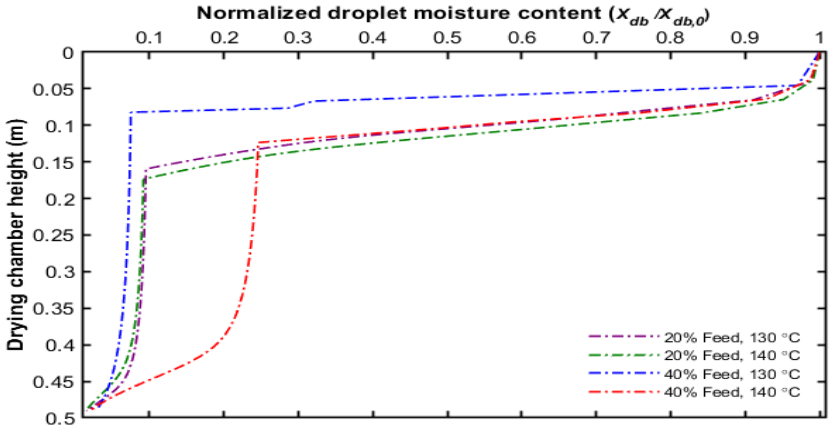

Figure 4: Model simulation results for normalised droplet moisture contents

Figure 5 and Figure 6 present the comparison between the predicted final moisture content from the simulation and the experimental data for the 20% and 40% w/w feed solids compositions, respectively, at drying air temperatures of 130 °C and 140 °C. The absolute percentage error between the model and experiment is shown on the secondary y-axis. The model accurately predicts the final powder moisture content, with absolute errors ranging from 2.3% to 5.2% for the 20% feed and from 1.0% to 1.8% for the 40% feed. The results confirm the expected trend: higher inlet drying air temperature enhances the rate of energy transfer to the droplets, promoting greater moisture evaporation and resulting in a lower final moisture content. The marginally higher error for the 20% solids feed is likely attributable to its higher initial stickiness

Corresponding author's email address: aliyub@unimaid.edu.ng

and greater propensity for wall deposition, a phenomenon not captured by the current model which assumes no wall interactions.

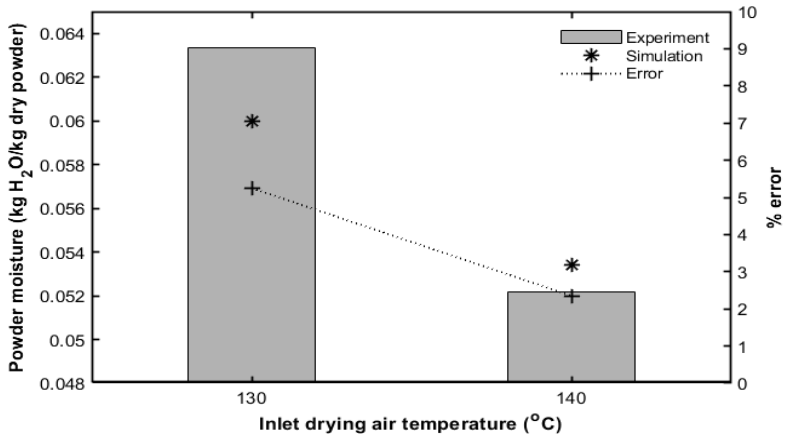

Figure 5: Comparison of juice powder moisture content from experiment and model for 20% feed

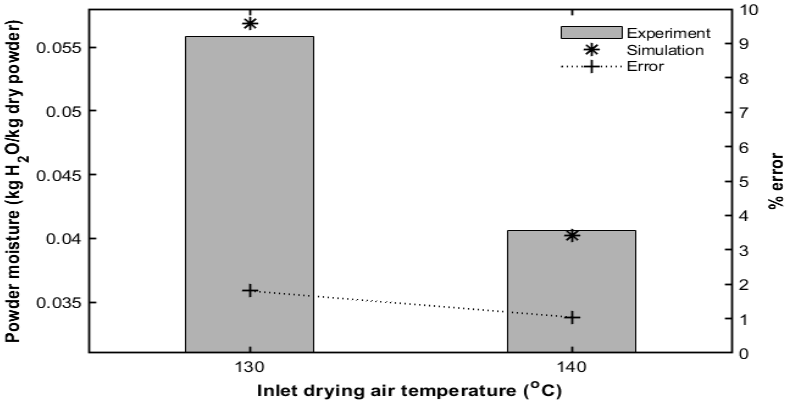

Figure 6: Comparison of juice powder moisture content from experiment and model for 40% feed

The predicted drying kinetics align quantitatively with the findings of Werner *et al.* (2008) for single sucrose droplets, who observed a similar transition to a receding interface model at a critical solids content. The absolute errors in final moisture content (1-5.2%) are comparable to or better than those reported for similar studies of food droplets (Putranto and Chen 2015), while this model retains the significant advantage of being based on fundamental physics rather than material-specific empirical parameters. This makes it more robust and potentially generalizable to a wider range of materials without the need for extensive new experimentation. The computational efficiency (average convergence in 28s) demonstrates that a high-fidelity, mechanistic model can be practically applied for process optimization and digital design, bridging a critical gap between oversimplified models and computationally expensive CFD approaches.

4. Conclusion

A deterministic mathematical model using advanced droplet vaporization kinetics and the receding interface-porous diffusion approach was developed and validated for simulating the spray drying of pineapple juice droplets. The model was validated using experimental data from pineapple juice spray drying at feed concentrations of 20% and 40% and drying temperatures of 130 °C and 140 °C. The model demonstrated strong predictive capability for final moisture content, with absolute errors between 1.0% and 5.2% across the varying feed concentrations and drying temperatures. More significantly, the model provided high-resolution, quantitative insights into the internal dynamics of drying, including the precise timing of crust formation (approx. 1.8 s), the evolution of internal temperature gradients (>40 °C), and the transition between drying periods. This study confirms that higher inlet drying air temperatures enhance moisture evaporation, leading to lower final moisture contents. This work demonstrates that the developed model effectively addresses a practical gap in the spray drying modelling. It provides a physically detailed, yet computationally efficient alternative to purely empirical models and resource-intensive CFD simulations. Its ability to accurately predict final powder properties while also revealing internal dynamics like crust formation and temperature gradients provides a powerful tool for fundamental research and industrial process optimization.

Corresponding author's email address: aliyub@unimaid.edu.ng

REFERENCES

Abramzon, B., and Sirignano, WA. 1989. Droplet vaporization model for spray combustion calculations. *International Journal of Heat and Mass Transfer*, *32*(9): 1605-1618.

Adhikari, B., Howes, T., Bhandari, BR., and Troung, V. 2003. Surface stickiness of drops of carbohydrate and organic acid solutions during convective drying: Experiments and modeling. *Drying Technology*, *21*(5): 839-873. https://doi.org/10.1081/drt-120021689

Akinsola, V. 2023. Numerical methods: Euler and runge-kutta. In *Qualitative and computational aspects of dynamical systems*. IntechOpen.

Ali, M., Mahmud, T., Heggs, PJ., Ghadiri, M., Djurdjevic, D., Ahmadian, H., Juan, LMd., Amador, C., and Bayly, A. 2014. A one-dimensional plug-flow model of a counter-current spray drying tower. *Chemical Engineering Research and Design*, *92*(5): 826-841. https://doi.org/10.1016/j.cherd.2013.08.010

American society of heating, RaA-CE. 2013. Psychrometrics. In *Handbook, ashrae fundamentals* (SI Edition ed.).

Barbosa-Cánovas, GV., Ortega-Rivas, E., Juliano, P., and Yan, H. (2006). *Food powders: Physical properties, processing and functionality*. Springer Science & Business Media.

Bell, IH., Wronski, J., Quoilin, S., and Lemort, V. 2014. Pure and pseudo-pure fluid thermophysical property evaluation and the open-source thermophysical property library coolprop. *Industrial and Engineering Chemistry Research*, *53*(6): 2498-2508. https://doi.org/10.1021/ie4033999

Bhattacharjee, A., and Gnanaskandan, A. 2023. Numerical simulation of particle evolution in spray drying using droplet drying kinetics. Heat Transfer Summer Conference, 2023. 87165 V001T007A003

Boel, E., Koekoekx, R., Dedroog, S., Babkin, I., Vetrano, MR., Clasen, C., and Van den Mooter, G. 2020. Unraveling particle formation: From single droplet drying to spray drying and electrospraying. *Pharmaceutics*, *12*(7): 625.

Camacho-Lie, M., Antonio-Gutiérrez, O., López-Díaz, AS., López-Malo, A., and Ramírez-Corona, N. 2023. Factors influencing droplet size in pneumatic and ultrasonic atomization and its application in food processing. *Discover Food*, *3*(1): 23.

Chen, XD., and Putranto, A. 2015. Reaction engineering approach (rea) to modeling drying problems: Recent development and implementations. *Drying Technology*, *33*(15-16): 1899-1910. https://doi.org/10.1080/07373937.2015.1069326

Feng, Z-G., and Michaelides, EE. 2001. Heat and mass transfer coefficients of viscous spheres. *International Journal of Heat and Mass Transfer*, *44*(23): 4445-4454. https://doi.org/10.1016/s0017-9310(01)00090-4

Filkova, I., Huang, LX., and Mujumdar, AS. 2014. Industrial spray drying systems. In *Handbook of industrial drying* (4th ed., pp. 191-226). CRC Press. https://doi.org/doi:10.1201/b17208-12

Gnielinski, V. 2010. G1 heat transfer in pipe flow. In *Vdi heat atlas* (pp. 691-700). Springer.

Gopireddy, SR., and Gutheil, E. 2013. Numerical simulation of evaporation and drying of a bi-component droplet. *International Journal of Heat and Mass Transfer*, *66*(0): 404-411. https://doi.org/10.1016/j.ijheatmasstransfer.2013.07.010

Herrmann, S., Kretzschmar, H-J., and Gatley, DP. 2011. Thermodynamic properties of real moist air, dry air, steam, water, and ice (rp-1485). *HVAC&R Research*, *15*(5): 961-986. https://doi.org/10.1080/10789669.2009.10390874

Kadja, M., and Bergeles, G. 2003. Modelling of slurry droplet drying. *Applied Thermal Engineering*, *23*(7): 829-844. https://doi.org/10.1016/s1359-4311(03)00014-0

Corresponding author's email address: aliyub@unimaid.edu.ng

Masters, K. (1991). *Spray drying handbook* (5th ed.). Longman Scientific & Technical.

Mezhericher, M., Levy, A., and Borde, I. 2007. Theoretical drying model of single droplets containing insoluble or dissolved solids. *Drying Technology*, *25*(6): 1025-1032. https://doi.org/10.1080/07373930701394902

Mezhericher, M., Levy, A., and Borde, I. 2010. Theoretical models of single droplet drying kinetics: A review. *Drying Technology*, *28*(2): 278-293. https://doi.org/10.1080/07373930903530337

Mezhericher, M., Levy, A., and Borde, I. 2014. Multi-scale multiphase modeling of transport phenomena in spray-drying processes. *Drying Technology*, *33*(1): 2-23. https://doi.org/10.1080/07373937.2014.941110

Michaelides, EES. 2013. Heat and mass transfer in particulate suspensions. Springer New York. https://books.google.com.my/books?id=YR8_AAAAQBAJ

Morrison, FA. 2013. An introduction to fluid mechanics. Cambridge University Press.

Pátek, J., Hrubý, J., Klomfar, J., Součková, M., and Harvey, AH. 2009. Reference correlations for thermophysical properties of liquid water at 0.1 mpa. *Journal of Physical and Chemical Reference Data*, *38*(1): 21-29. http://dx.doi.org/10.1063/1.3043575

Poozesh, S., Lu, K., and Marsac, PJ. 2018. On the particle formation in spray drying process for bio-pharmaceutical applications: Interrogating a new model via computational fluid dynamics. *International Journal of Heat and Mass Transfer*, *122*: 863-876.

Putranto, A., and Chen, XD. 2015. An assessment on modeling drying processes: Equilibrium multiphase model and the spatial reaction engineering approach (s-rea). *Chemical Engineering Research and Design*, *94*: 660-672. https://doi.org/10.1016/j.cherd.2014.10.007

Razmi, R., Jubaer, H., Krempski-Smejda, M., Jaskulski, M., Xiao, J., Chen, XD., and Woo, MW. 2021. Recent initiatives in effective modeling of spray drying. *Drying Technology*, *39*(11): 1614-1647.

Rezaei, M., and Netz, RR. 2021. Water evaporation from solute-containing aerosol droplets: Effects of internal concentration and diffusivity profiles and onset of crust formation. *Physics of Fluids*, *33*(9).

Sadafi, MH., Jahn, I., Stilgoe, AB., and Hooman, K. 2014. Theoretical and experimental studies on a solid containing water droplet. *International Journal of Heat and Mass Transfer*, *78*: 25-33. https://doi.org/10.1016/j.ijheatmasstransfer.2014.06.064

Sazhin, S., Elwardany, AE., Gusev, IG., Xie, J., Shishkova, I., Cao, B-Y., and Heikal, M. 2013. New models for droplet heating and evaporation. *Asian Journal of Scientific Research*, *6*(2): 177-186.

Sazhin, SS. 2006. Advanced models of fuel droplet heating and evaporation. *Progress in Energy and Combustion Science*, *32*(2): 162-214. https://doi.org/10.1016/j.pecs.2005.11.001

Sazhin, SS. 2014. Droplets and sprays (Vol. 63). Springer.

Sazhin, SS., Elwardany, AE., Krutitskii, PA., Deprédurand, V., Castanet, G., Lemoine, F., Sazhina, EM., and Heikal, MR. 2011. Multi-component droplet heating and evaporation: Numerical simulation versus experimental data. *International Journal of Thermal Sciences*, *50*(7): 1164-1180. https://doi.org/10.1016/j.ijthermalsci.2011.02.020

Semenova, M., Vasileva, A., Lukina, G., and Popova, U. 2021. Solving differential equations by means of mathematical simulation in simulink app of matlab software package. In *Technological advancements in construction: Selected papers* (pp. 417-431). Springer.

Werner, SRL., Edmonds, RL., Jones, JR., Bronlund, JE., and Paterson, AHJ. 2008. Single droplet drying: Transition from the effective diffusion model to a modified receding interface model. *Powder Technology*, *179*(3): 184-189. https://doi.org/10.1016/j.powtec.2007.06.009

Corresponding author's email address: aliyub@unimaid.edu.ng